Autonomously Aided Strapdown Attitude Reference System

M. Koifman* and S. J. Merhav†
Technion—Israel Institute of Technology, Technion City, Haifa, 32000 Israel

The feasibility of an autonomously aided strapdown attitude reference system, based solely on the measurements of an orthogonal triad of rate gyros and conventional air data, is explored. The aiding is provided by the aerodynamic model of the aircraft and a reduced-order multirate extended Kalman filter (EKF). It is demonstrated that the EKF provides on-line attitude estimates with bounded errors not exceeding 0.5 deg at output rates on the order of 20 Hz. On-line simulation tests, incorporating low-cost rate gyros mounted on a high-precision three-axis flight table, validate the feasibility of the concept.

Introduction

THE work described herein is motivated, among others, by the continuing need for an autonomous, small and reliable attitude reference system, particularly in the growing field of remotely piloted vehicles (RPVs), in which the use of solid-state miniature rate sensors is anticipated. The current state of the art in the determination of aircraft attitude angles is still primarily by means of the vertical gyroscope (see, for example, Ref. 1). It is gravity controlled to avoid unbounded drift, but, consequently, it is acceleration sensitive. It is generally bulky, has limited angular freedom, and is of relatively low reliability. The other established approach is by strapdown inertial measurement technology (see, for example, Ref. 2), in which the outputs of a triad of body-mounted rate gyros are integrated by the Euler equations, or quaternions, to provide aircraft attitude angles. It is neither gravity controlled, nor acceleration sensitive, but it has unbounded drift, unless external aiding is used. To achieve satisfactory precision over periods of several hours, costly inertial-grade rate gyros are required. A blend of preceding methods is described in Ref. 3, which, essentially, is a strapdown mechanization of a vertical gyro using a good-quality two-axis dry tuned rotor gyro,[4] and, in addition, two accelerometers for gravity control to assure bounded drift. Yet, it is acceleration sensitive as is the vertical gyro. A number of attempts to provide low-cost attitude information derived from the geophysical environment have been reported. For example, Hill[5] proposed a capacitive method by using the electrostatic field near the Earth. Pietila and Dunn[6] proposed a triad of magnetometers using the Earth's magnetic field. These approaches have not matured as practical technologies apparently because of sensitivity to interferences. Bryson[7] indicated the possibility of determining attitude angles by means of angular rate measurements and a linear fixed-gain Kalman filter based on a linearized model of the aircraft in straight-and-level flight. He did not extend this study for maneuvering aircraft with widely varying altitude- and relative airspeed. Grunwald et al.[8] initially investigated this concept for maneuvering aircraft using a linearized model and a constant-gain Kalman filter to avoid computational load, and found substantial errors in attitude estimation. Even with a complete nonlinear aerodynamic model and a constant-gain extended Kalman filter, these errors were not sufficiently reduced.

Received Oct. 31, 1989; revision received June 8, 1990; accepted for publication July 2, 1990.

*Graduate Student, Department of Aerospace Engineering.

†Professor, Department of Aerospace Engineering; currently on leave at NASA Ames Research Center, Mail Stop 210-9, Moffet Field, CA 94035.

The conclusion was that a variable-gain extended Kalman filter (EKF) is necessary, and the challenge was to implement it for real-time operation. The use of an EKF for maneuvering aircraft as part of an off-line algorithm for the identification of aerodynamic coefficients is described in Ref. 9. However, real-time implementation was not an objective, and it would not have been feasible because of the large dimensions of the state and measurement vectors. This paper describes a feasibility study of determining aircraft attitude angles using an EKF based on the complete nonlinear aerodynamic equations, the primary measurements of low-cost rate gyros with time-varying biases on the order of 0.1 deg/s, magnetic heading and the secondary standard measurements of relative airspeed and barometric altitude for updating aerodynamic parameters, and magnetic heading. The main points in this study are:

1) To find a computationally economic formulation of the EKF that provides the estimates of attitude angles with a precision better than 1 deg and that operates at rates of at least 20 Hz to satisfy the needs for flicker-free display and smooth control.

2) To investigate the effect of rate gyro biases on the attitude estimation error and to devise a method for coping with their time-varying nature.

3) To study the effects of uncertainties of the aircraft aeromechanical parameters and of atmospheric turbulence on the attitude estimation errors.

Results are presented in accordance with the foregoing points. They are demonstrated by detailed off-line computer simulations and validated by on-line laboratory "flight tests" using rate gyros and a high-precision computer-controlled three-axis flight table. The results indicate very good performance under diversified flight conditions, maneuvers, variations in aeromechanical parameters, and time-varying gyro biases.

System Modeling

Aircraft Atmospheric Turbulence and Sensors

Aircraft motion is described by 12 standard equations given in Appendix A.

Atmospheric turbulence is described by a vector velocity field $[u_g, v_g, w_g]^T$, where the subscript g indicates gust and is modeled after Dryden[10] and formulated as an airspeed- and altitude-dependent first-order Gauss-Markov process with an unknown mean value.

The measurement system consists of 1) a triad of orthogonally body-mounted rate gyros for the measurement of pitch rate q, roll rate p, and yaw rate r; 2) a magnetic heading sensor for measuring ψ; 3) an airspeed sensor; and 4) a barometric altimeter. All measurements are contaminated by random noise and unknown biases.

Extended Kalman Filter Formulation and Performance

The state vector of the aircraft as defined by Eqs. (A1-A10) can be augmented by the variables describing the atmospheric turbulence and the gyro biases. Thus, in the nonlinear state-space equation

$$X(t) = f[X(t), U(t)] + W(t) \tag{1}$$

$X(t) \in R^{16}$ is the augmented state vector defined by

$$X(t) \triangleq [u, v, w, p, q, r, \phi, \theta, \psi, h, u_g, v_g, w_g, \mu_p, \mu_q, \mu_r]^T$$

The first 10 terms in this vector are the aircraft state variables, the next three are the gust components, and the last three are the gyro biases that are important in obtaining good estimates of aircraft attitude, especially with low-grade rate gyros. Initially, it is assumed that $\dot{\mu}_p = \dot{\mu}_q = \dot{\mu}_r = 0$, i.e., that gyro biases are unknown constants. The case with time varying drift rates will be addressed subsequently.

$U(t) \in R^4$ is the control vector defined by:

$$U(t) \triangleq [\delta_e, \delta_a, \delta_r, \delta_T]^T$$

where the four elements stand for elevator, aileron, rudder, and throttle, respectively.

$W(t) \in R^{16}$ is a vector of continuous white noise defined by

$$W(t) \triangleq [0, 0, 0, 0, 0, 0, 0, 0, 0, 0, w_1, w_2, w_3, 0, 0, 0]^T$$

The measurement equation is

$$Z_k = HX_k + V_k \tag{2}$$

where

$$Z_k \triangleq [V_m, p_m, q_m, r_m, \psi_m, h_m]^T$$

The index k indicates that the estimated variable is given at the instant t_k; m indicates measured quantities; and H is the measurement matrix defined by

$$H \triangleq \begin{bmatrix} 1 & 0 & 0 & 0 & 0 & 0 & 0 & 0 & 0 & 0 & -1 & 0 & 0 & 0 & 0 & 0 \\ 0 & 0 & 0 & 1 & 0 & 0 & 0 & 0 & 0 & 0 & 0 & 0 & 0 & 1 & 0 & 0 \\ 0 & 0 & 0 & 0 & 1 & 0 & 0 & 0 & 0 & 0 & 0 & 0 & 0 & 0 & 1 & 0 \\ 0 & 0 & 0 & 0 & 0 & 1 & 0 & 0 & 0 & 0 & 0 & 0 & 0 & 0 & 0 & 1 \\ 0 & 0 & 0 & 0 & 0 & 0 & 0 & 0 & 1 & 0 & 0 & 0 & 0 & 0 & 0 & 0 \\ 0 & 0 & 0 & 0 & 0 & 0 & 0 & 0 & 0 & 1 & 0 & 0 & 0 & 0 & 0 & 0 \end{bmatrix}$$

$V_k \in R^6$ is a vector of discrete white noise defined by

$$V \triangleq [V_v, V_p, V_q, V_\gamma, V_\psi, V_h]^T$$

Equations (1) and (2) permit formulation of an EKF. Its algorithm is given in Appendix B in accordance with Ref. 11. A series of computer simulations was performed. The aircraft chosen as a model was a slow, subsonic, conventionally configured RPV. Figure 1 shows an example of a 300-s run with initial values of velocity of 40 m/s, initial altitude of 1000 m, and atmospheric turbulence with 1-m/s rms. The simulation was performed with an aircraft in open loop without control surface activity. Since the aircraft has unstable lateral dynamics, it executes a spiral dive, as indicated by Fig. 1. Under these conditions, all of the parameters of the aircraft undergo extreme variations. Yet, the estimation errors of the attitude angles converge to less than 0.1 deg. Figure 1 shows the performance for the roll angle ϕ. Similar results hold for θ and ψ. Additional simulation runs were performed for a variety of maneuvers and different conditions of atmospheric turbulence yielding similar results.

The foregoing implies that the aircraft parameters are known. Since substantial uncertainties in these parameters normally exist, their effect on the precision of the attitude estimates was investigated. These uncertainties were assumed to be on the order of 5%, which is a reasonable state-of-the-art assumption. The effects of variations of every aerodynamic coefficient were investigated separately by flight simulations in both straight-and-level flight and "slalom" maneuvers at 5000 m altitude and airspeed of 40 m/sec. For each run, a deviation of a different parameter in the model was assumed. The results disclosed that the algorithm can tolerate parameter deviations up to 5%. In all cases, attitude estimation errors did not exceed 1 deg. The largest sensitivity was found to be with respect to the lift slope coefficient $C_{L\alpha}$, assumed to be a constant for moderate values of α. However, this coefficient is relatively well known and its uncertainty is small. Effects of uncertainty in control derivatives can be interpreted as deviations in stability derivatives. Trim offsets are canceled by the control system and do not affect the EKF. Clearly, the algorithm can operate only after the aircraft becomes airborne, because only then can the equations of motion on which the estimator is based become valid. Therefore, initially, and for a short time before takeoff, the attitude angles are directly determined by integrating the rate gyro outputs by the Euler equations. Initial errors, which may accumulate, vanish because the estimator converges to the real attitude angles of the aircraft.

Real-Time Implementation of Extended Kalman Filter

With $X \in R^{16}$, the implementation of the EKF for on-line operation is not feasible. Examination of the computing rate disclosed that one cycle of computation requires about 1 s of CPU time on a VAX 750, whereas the propagation of the estimated state vector must be carried out with a step not greater than 10 ms to assure numerical stability. To achieve a drastic reduction in this 100:1 ratio for on-line operation, the following steps were taken.

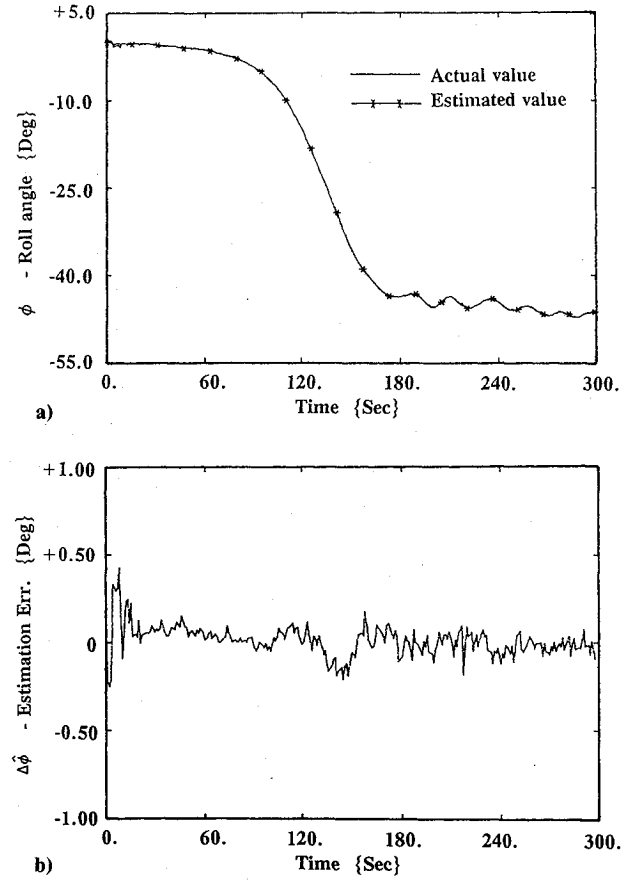

Fig. 1 Time history of a) roll angle ϕ and its estimate $\hat{\phi}$, and b) estimation error $\Delta\hat{\phi}$ using the full-order EKF in noncontrolled flight.

Reduction of the Dimension of State Vector X

1) Remove the altitude h from the state vector X and h_m from the measurement vector Z but use the barometric measurement h_m directly for computing air density to update aerodynamic parameters.

2) Remove the azimuth ψ from the state vector. The estimator cannot provide more accurate values of ψ than the compass itself because no provision exists in the present formulation for estimating azimuth errors.

3) Estimate relative airspeed resolved in body coordinates as follows:

$$u_R = u - u_g \tag{3a}$$

$$v_R = v - v_g \tag{3b}$$

$$w_R = w - w_g \tag{3c}$$

Consequently, the reduced order state and measurement vectors are:

$$X \triangleq [\mu_p,\ \mu_q,\ \mu_r,\ p,\ q,\ r,\ u_R,\ v_R,\ w_R,\ \phi,\ \theta]^T \tag{4}$$

and

$$Z \triangleq [p_m,\ q_m,\ r_m,\ V_m]^T \tag{5}$$

Simplification of Computations

Substantial saving in computational effort is achieved by the discrete propagation of the estimation error covariance matrix P. Its propagation is executed by the solution of Eq. (B2). To ensure numerical stability, a very small step must be used, which implies a slow rate of integration. More accurate algorithms, such as Runge-Kutta, permit the use of large steps but increase computational complexity. To circumvent this conflict, the discrete formulation of Eq. (B2), which actually is its solution, was chosen, i.e.,

$$P_{k+1|k} = \Phi(\hat{X},U,\Delta t)P_{k|k}\Phi^T(\hat{X},U,\Delta t) + \tilde{Q}(\Delta t) \tag{6}$$

where Φ is the transition matrix of the differential equation $\partial\Phi/\partial t = F\Phi$; it can be computed by the equation

$$\Phi(\hat{X},U,\Delta t) = \exp\{F(\hat{X},U)\Delta t\} = \sum_{n=0}^{\infty} \frac{\{F(X,U)\Delta t\}^n}{n!} \tag{7}$$

Define $\tilde{Q}$ as the process noise covariance matrix defined by

$$\tilde{Q}(\Delta t) = \int_0^{\Delta t} \Phi(\hat{X},U,\tau)Q(\tau)\Phi^T(X,U,\tau)\,d\tau \tag{8}$$

By neglecting terms of order equal to or greater than Δt^2, one can use the approximation

$$\tilde{Q} \sim Q\Delta t \tag{9}$$

Using the special form of Φ and the symmetry of the covariance matrix, computational complexity can be substantially reduced. By partitioning Φ into submatrices, Φ can be written in the following form:

$$\Phi(\hat{X},U,\Delta t) = \begin{bmatrix} I & 0 & 0 \\ 0 & \Phi_{11} & \Phi_{12} \\ 0 & \Phi_{21} & \Phi_{22} \end{bmatrix} \tag{10}$$

Φ_{11}, Φ_{12}, Φ_{21}, and Φ_{22} are 4×4 submatrices, and I is a 3×3 identity matrix that results from the augmentation of the state vector by the three biases of the gyros. The state estimation error covariance matrix P is symmetrical, and it can be partitioned into submatrices as follows:

$$P = \begin{bmatrix} P_{11} & P_{12} & P_{13} \\ P_{12}^T & P_{22} & P_{23} \\ P_{13}^T & P_{23}^T & P_{33} \end{bmatrix} \tag{11}$$

where P_{11} is a 3×3 submatrix; P_{12} and P_{13} are 3×4 submatrices; and P_{22}, P_{23}, and P_{33} are (4×4) submatrices.

$\tilde{Q}$, the process noise covariance matrix, can be partitioned into submatrices as follows:

$$\tilde{Q} = \begin{bmatrix} 0 & 0 & 0 \\ 0 & \tilde{Q}_1 & 0 \\ 0 & 0 & \tilde{Q}_2 \end{bmatrix} \tag{12}$$

$\tilde{Q}_1$ and $\tilde{Q}_2$ are 4×4 submatrices. Using Eqs. (10–12), Eq. (6) can be rewritten to obtain explicit equations for the propagation of the state error covariance matrix P as follows:

$$[P_{11}]_{k+1|k} = [P_{11}]_{k|k} \tag{13a}$$

$$[P_{12}]_{k+1|k} = [P_{12}]_{k|k}\Phi_{11}^T + [P_{13}]_{k|k}\Phi_{12}^T \tag{13b}$$

$$[P_{13}]_{k+1|k} = [P_{12}]_{k|k}\Phi_{21}^T + [P_{13}]_{k|k}\Phi_{22}^T \tag{13c}$$

$$[P_{22}]_{k+1|k} = \Phi_{11}[P_{22}]_{k|k}\Phi_{11}^T + \Phi_{11}[P_{23}]_{k|k}\Phi_{12}^T + \{\Phi_{11}[P_{23}]_{k|k}\Phi_{12}^T\}^T + \Phi_{12}[P_{33}]_{k|k}\Phi_{12}^T + \tilde{Q}_1 \tag{13d}$$

$$[P_{23}]_{k+1|k} = \Phi_{11}[P_{22}]_{k|k}\Phi_{21}^T + \Phi_{11}[P_{23}]_{k|k}\Phi_{22}^T + \{\Phi_{21}[P_{23}]_{k|k}\Phi_{12}^T\}^T + \Phi_{12}[P_{33}]_{k|k}\Phi_{22}^T \tag{13e}$$

$$[P_{33}]_{k+1|k} = \Phi_{21}[P_{22}]_{k|k}\Phi_{21}^T + \Phi_{21}[P_{23}]_{k|k}\Phi_{22}^T + \{\Phi_{21}[P_{23}]_{k|k}\Phi_{22}^T\}^T + \Phi_{22}[P_{33}]_{k|k}\Phi_{22}^T + \tilde{Q}_2 \tag{13f}$$

Exploiting the sparseness of the measurement equation and using the fact that H consists only of zeros and units, a substantial amount of operations can be saved, since the product of H by another matrix only requires summations with elements of the other matrix without the need for multiplications.

After the reduction of X and Z to dimensions 11 and 4, respectively, H takes on the form

$$H = \left[\begin{array}{ccc|cccc|cccc} 1 & 0 & 0 & 1 & 0 & 0 & 0 & 0 & 0 & 0 & 0 \\ 0 & 1 & 0 & 0 & 1 & 0 & 0 & 0 & 0 & 0 & 0 \\ 0 & 0 & 1 & 0 & 0 & 1 & 0 & 0 & 0 & 0 & 0 \\ 0 & 0 & 0 & 0 & 0 & 0 & 1 & 0 & 0 & 0 & 0 \end{array}\right] \tag{14}$$

H can be written as:

$$H = [C \mid I \mid 0] \tag{15}$$

C is 4×3; I is 4×4; and 0 is 4×4. Substituting Eqs. (15) and (11) into Eq. (B4), we obtain the following equations for computing the gains:

$$[K_1]_{k+1} = G_1M^{-1} \tag{16a}$$

$$[K_2]_{k+1} = G_2M^{-1} \tag{16b}$$

$$[K_3]_{k+1} = G_3M^{-1} \tag{16c}$$

where K_1 (3×4), K_2 (4×4), and K_3 (4×4) are submatrices of the overall (11×4) gain matrix K, and where G_1, G_2, and G_3 are given by the following relationships:

$$G_1 = [P_{11}]_{k+1|k}C^T + [P_{12}]_{k+1|k} \tag{17a}$$

$$G_2 = [P_{12}]_{k+1|k}C^T + [P_{22}]_{k+1|k} \tag{17b}$$

$$G_3 = [P_{13}]^T_{k+1|k}C^T + [P_{23}]_{k+1|k} \tag{17c}$$

and M is given by:

$$M = C[P_{11}]_{k+1|k}C^T + C[P_{12}]_{k+1|k} + \{C[P_{12}]_{k+1|k}\}^T + R \quad (18)$$

It is also advantageous to use the special form of H to reduce the computational complexity when updating the estimation error covariance matrix P. Substituting Eqs. (14) and (15) into Eq. (B7), we derive

$$[P_{11}]_{k+1|k+1} = [P_{11}]_{k+1|k} - G_1[K_1]^T_{k+1} - \{G_1[K_1]^T_{k+1}\}^T + [K_1]_{k+1}M[K_1]^T_{k+1} \quad (19a)$$

$$[P_{12}]_{k+1|k+1} = [P_{12}]_{k+1|k} - G_1[K_2]^T_{k+1} - [K_1]_{k+1}G_2^T + [K_1]_{k+1}M[K_2]^T_{k+1} \quad (19b)$$

$$[P_{13}]_{k+1|k+1} = [P_{13}]_{k+1|k} - G_1[K_3]^T_{k+1} - [K_1]_{k+1}G_3^T + [K_1]_{k+1}M[K_3]^T_{k+1} \quad (19c)$$

$$[P_{22}]_{k+1|k+1} = [P_{22}]_{k+1|k} - G_2[K_2]^T_{k+1} - \{G_2[K_2]^T_{k+1}\}^T + [K_2]_{k+1}M[K_2]^T_{k+1} \quad (19d)$$

$$[P_{23}]_{k+1|k+1} = [P_{23}]_{k+1|k} - G_2[K_3]^T_{k+1} - [K_2]_{k+1}G_3^T + [K_2]_{k+1}M[K_3]^T_{k+1} \quad (19e)$$

$$[P_{33}]_{k+1|k+1} = [P_{33}]_{k+1|k} - G_3[K_3]^T_{k+1} - \{G_3[K_3]^T_{k+1}\}^T + [K_3]_{k+1}M[K_3]^T_{k+1} \quad (19f)$$

The propagation of the covariance matrix P in time requires the linearization of the nonlinear equations of motion of the aircraft in order to derive the Jacobian F and the computation of the transition matrix Φ. The use of the original algorithm of the EKF requires the computation of the matrices F and Φ in each computational cycle, thus causing very large computational load. However, the dynamics of the aircraft model indicate that the fastest modes, roll subsidence, dutch roll, and short-period pitch are on the order of 1 s. Since the linearization for obtaining F is done in the neighborhood of $\hat{x}_{k+1|k}$, and with the assumption that $\hat{x}_{k+1|k} \rightarrow x_{k+1}$, it is not necessary to compute F and, thus, Φ at a rate greater than a few times per second, i.e., a much slower rate than the 10 ms required in the original EKF. A high rate of computation does not contribute to precision because the difference between Φ_k and Φ_{k+1} is negligible.

Implementation of Reduced-Order Extended Kalman Filter

The reduced-order EKF with the foregoing computational simplifications was implemented in a VME Motorola System 1131.

Tests of this algorithm disclosed that the cycle time of the EKF was 0.111 s. Using this relatively large time interval as an integration step would cause numerical divergence. To effectively reduce the integration time, the filter was implemented by means of a multirate scheme, using two separate computation rates, so that F and Φ were not computed in every cycle. Consequently, the resulting algorithm operated in real time at a rate of 16 Hz, with its cycle periods consisting of the following operations.

The first cycle consists of:

1) Propagation of the state vector X in accordance with Eq. (B1).

2) Computation of the Jacobian F in accordance with Eq. (B3).

3) Computation of the transition matrix Φ in accordance with Eq. (7) using only the first three terms in the series.

4) Propagation of the covariance matrix P in accordance with Eq. (13).

The second cycle consists of:

1) Propagation of the state vector X in accordance with Eq. (B1).

2) Propagation of the estimation error covariance matrix P in accordance with Eq. (13) in which Φ, computed in the first cycle, is used.

3) Computation of the gain matrix K in accordance with Eqs. (17).

4) Updating the state vector X in accordance with Eq. (B5).

5) Updating the estimation error covariance matrix P in accordance with Eq. (19).

The second cycle is executed five times, after which the computation in the first cycle is resumed, and so on. This 5:1 ratio was determined by tuning the filter and by simulation, and it represents a good compromise between the need to reduce the update interval of the transition matrix Φ and the need to increase the output rate of the EKF. A block diagram describing the filter is shown in Fig. 2.

Computer Simulations of Reduced-Order Extended Kalman Filter

Extensive computer simulations were carried out to evaluate the performance of this reduced-order on-line filter. Figure 3 describes a 600-s sample of a simulation run for initial flight conditions of 40 m/s, 1000-m altitude, and atmospheric turbulence of 1-m/s rms. The aircraft was "flown" in open loop, i.e., without control surface activity. These are the same flight conditions underlying Fig. 1. Comparison of Figs. 1 and 3

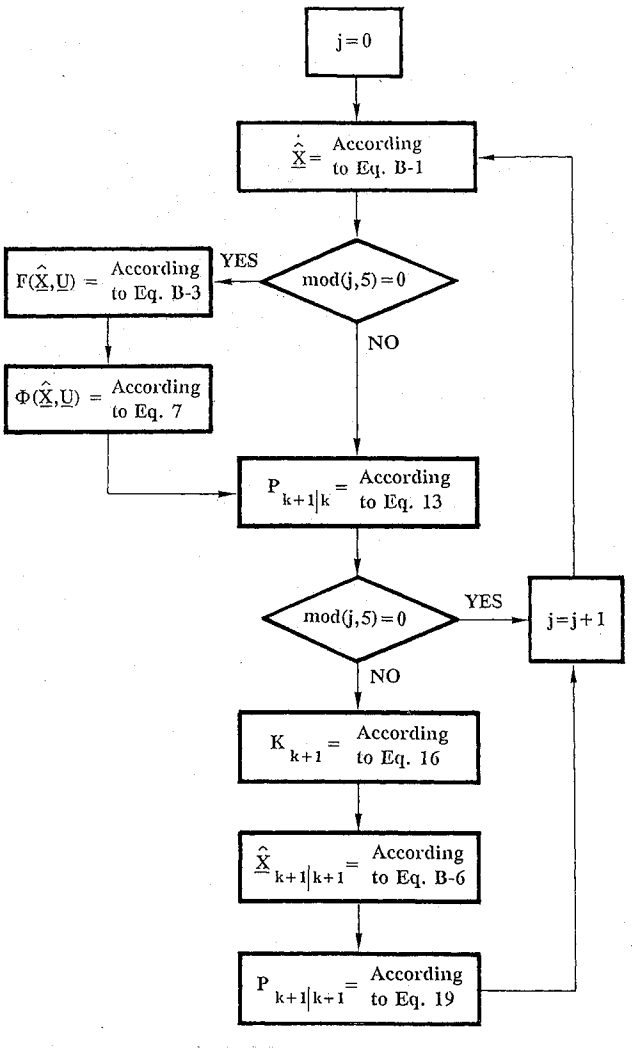

Fig. 2 Block diagram of reduced-order EKF.

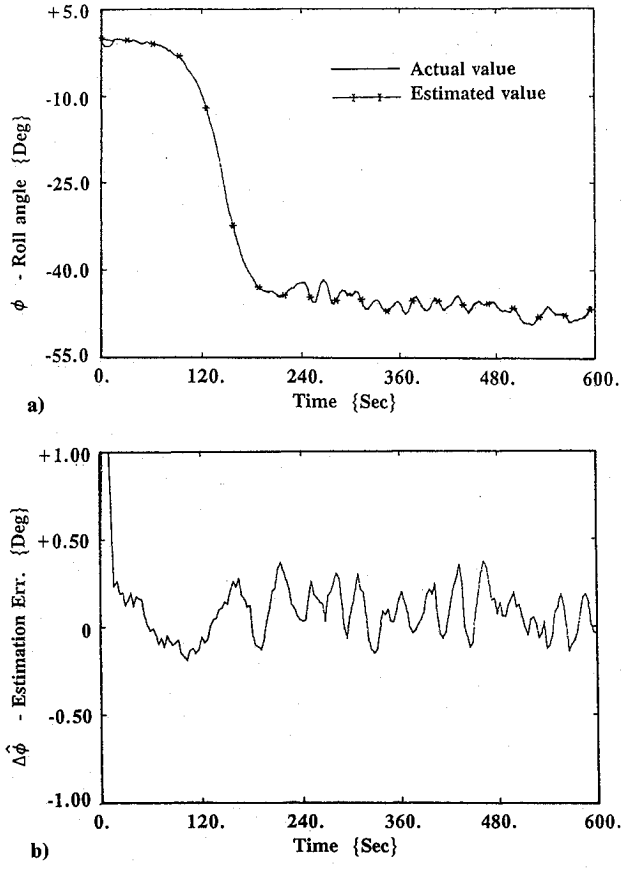

Fig. 3 Time history of a) roll angle ϕ and its estimate $\hat{\phi}$, and b) estimation error $\Delta\hat{\phi}$ using the reduced-order EKF in noncontrolled flight.

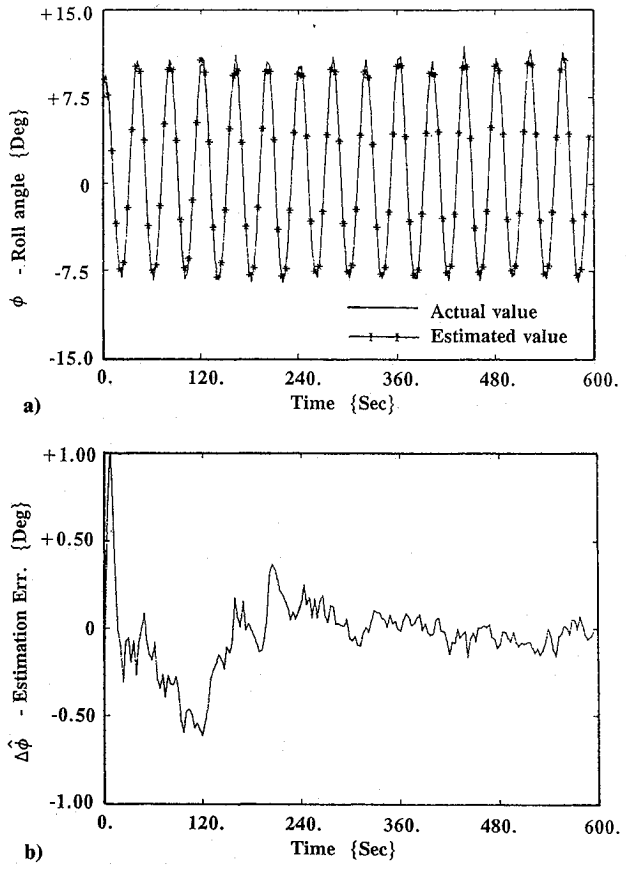

Fig. 4 Time history of a) roll angle ϕ and its estimate $\hat{\phi}$, and b) estimation error $\Delta\hat{\phi}$ using the reduced-order EKF in a "slalom" flight.

shows that the estimation error of the reduced order-filter is larger, but its accuracy and rate are quite compatible with typical requirements in aircraft flight control. The standard deviations for the ϕ and θ estimation errors are $\sigma_{\Delta\hat{\phi}} = 0.21$ deg and $\sigma_{\Delta\hat{\theta}} = 0.26$ deg, respectively (the latter not shown). Figure 4 shows a simulation run of a "slalom" trajectory in which ϕ and θ vary periodically with a period of 40 s and amplitudes of 10 and 15 deg, respectively. The results demonstrate that the convergence time of the reduced-order EKF is somewhat longer than for the full-state EKF. However, its sensitivity to the effects of aircraft parameter variations is substantially smaller. Simulations, with conditions identical to those of Figs. 3 and 4, were also performed in which the F and Φ matrices were computed in each cycle at a 16-Hz rate, which did not permit real-time operation. The results obtained were very similar to those in Figs. 3 and 4. This justifies the assumption that it is not necessary to compute Φ and F in each cycle. In the present example, the rate gyros were assumed to have drift rate biases on the order of 0.1 deg/s, which would cause offsets in the attitude estimates in excess of 1 deg. Therefore, gyro biases were included in the Kalman filter. However, additional simulations disclosed that biases smaller than 0.03 deg/s result in negligible attitude estimation errors. Thus, for this class of gyros, estimation of biases is not needed. This would result in additional reduction of the order of the filter from 11 to 8, implying a very significant savings in computation time.

Realization of Extended Kalman Filter with Time-Varying Gyro Biases

So far, it has been assumed that the gyro drift rate can be modeled as unknown constants. In reality, this is not the case. Furthermore, it is not feasible to formulate a mathematical model for the biases in low-grade rate gyros because of nonlinearities, hysteresis, and mechanical uncertainties that cause erratic jumps in the biases. Accordingly, they have been modeled as piecewise-constant random processes. Since the EKF, as described so far, is based on constant drift rates, it cannot estimate variations in biases that are subsequent to their initial estimates because the corresponding components in the gain vector would have converged to zero.

To implement an EKF that maintains alertness to possible variations in gyro biases and continues to estimate them indefinitely, the following approach is adopted: the biases continue to be modeled as constants, but, to prevent the corresponding gains from converging to zero, the diagonal elements due to drift rates in the estimation error covariance matrix P are reinitialized from time to time. This reinitialization should be enforced whenever a significant change in the bias occurs. This implies a detector that is sensitive to such variations. A suitable scheme was proposed by Hinkley[12] and Basseville.[13] For its implementation, we define a new variable Y as

$$Y_k \triangleq \omega_{mk} - \hat{\omega}_k - \hat{\mu}_k \tag{20}$$

where ω_m is the actual gyro output, $\hat{\omega}$ the estimated angular rate, and $\hat{\mu}$ the estimated drift. It is assumed that in the steady state, i.e., after the decay of transients, $\hat{\omega} \to \omega_k$ and $\hat{\mu} \to \mu_k$, so that

$$E[Y_k] = E[\omega_{mk} - \hat{\omega}_k - \hat{\mu}_k] \simeq E[V_k] = 0 \tag{21}$$

Assume that at a given instant t_k, a change in the bias occurs. This can be formulated by:

$$\mu_k = \mu_o, \qquad t < t_k$$

$$\mu_k = \mu_o + \Delta\mu, \qquad t \geq t_k \tag{22}$$

Therefore, after the event of the change, we have,

$$E[Y_k] = \Delta\mu \tag{23}$$

This change in $E[Y_k]$ is an indication of a change in the bias. The detection algorithm can, therefore, be formulated as follows. A threshold value μ_t is chosen and two algorithms operate in parallel, one to detect an increase, and the other to detect a decrease in $E[Y_k]$:

$$T_o = 0 \tag{24a}$$

$$T_n = T_{n-1} + Y_n + \Delta\mu_m/2 \tag{24b}$$

$$M_n = \max_{1 \le k \le n} T_k \tag{24c}$$

$$M_n - T_n \ge \lambda \tag{24d}$$

Alarm, if $M_n - T_n \ge \lambda$

$$U_o = 0 \tag{25a}$$

$$U_n = U_{n-1} + Y_n - \Delta\mu_m/2 \tag{25b}$$

$$N_n = \min_{1 \ge k \ge n} U_k \tag{25c}$$

$$U_n - N_n \ge \lambda \tag{25d}$$

Alarm, if $U_n - N_n \ge \lambda$.

λ is a threshold value, the choice of which is a compromise between too many false alarms if λ is set too small and too many undetected changes in drift rate if λ is set too large. λ is determined by the following relation:

$$\lambda = \gamma(\sigma^2/\Delta\mu_m/2) \tag{26}$$

where σ is the standard deviation of the measurement noise V_k and γ a constant suitably chosen to be between 3 and 5.

The results of simulations with randomly occurring variations in gyro drift rates confirmed that the Hinkley[12] detector solves the problem of estimating time-varying biases and it is effective for continuous random variations as well.

Experimental Validation

Experimental Setup

The experimental setup used for validation of the method consisted of the following subsystems and parts:

1) A high-precision, digitally controlled three-axis flight table with bandwidths of 7, 10, and 15 Hz for the yaw, pitch, and roll gimbals, respectively, for small amplitudes of less than a degree. The flight table and its digital controller are depicted in Fig. 5.

2) A communication board interfacing the computer and the flight table. This board is based on a 8-MHz MC68010 CPU and three analog-to-digital 12-bit converters that sample the readings of the three rate gyros.

3) A Motorola VME System 1131 computer based on a 16-MHz CPU MC68020 and a floating-point unit, MC68881.

4) Three dc to dc Condor Pacific deflection-type rate gyros, Model RB43BD with a measurement range of 100 deg/s.

Real Time Simulation Tests with Rate Gyros

The real-time simulations for the estimation of attitude angles were executed in accordance with Fig. 6. The flight simulations of the trajectories and sensor readings were performed off-line and stored in files. These were subsequently used in the real-time simulations as inputs to the EKF. In the process of tuning the EKF, the values for the process noise covariance matrix $\tilde{Q} \in \Re^{11\times 11}$ and the measurement covariance matrix $R \in \Re^{4\times 4}$ were found to be $\tilde{Q}(7,7) = \tilde{Q}(8,8) = \tilde{Q}(9,9) = 0.229\ \text{m}^2/\text{s}^2$, and all other elements of $\tilde{Q}$ are zero. $R(1,1) = R(2,2) = R(3,3) = 1.2 \times 10^{-4}\ (\text{rad/s})^2$, $R(4,4) = 0.9\ (\text{m/s})^2$, and all other elements of R are zero. Figure 7 displays simulation results for an uncontrolled aircraft during a spiral dive. The flight conditions are identical to those underlying Fig. 1 and those of Fig. 3 which represented computer simulations with analytical models of the gyros. In those simulations, imperfections of the flight table did not play a role. The errors are somewhat larger than those in Fig. 3, e.g., $\hat{\sigma}_{\Delta\phi} = 0.32$ deg and $\hat{\sigma}_{\Delta\Theta} = 0.35$ deg. Increased error results from the imperfections of the dynamics of the flight table and the nonlinearities of the actual rate gyros. Yet, with all of the shortcomings of the experimental test, the estimation errors in pitch and roll did not exceed 0.5 deg. Figure 8 describes the results of a

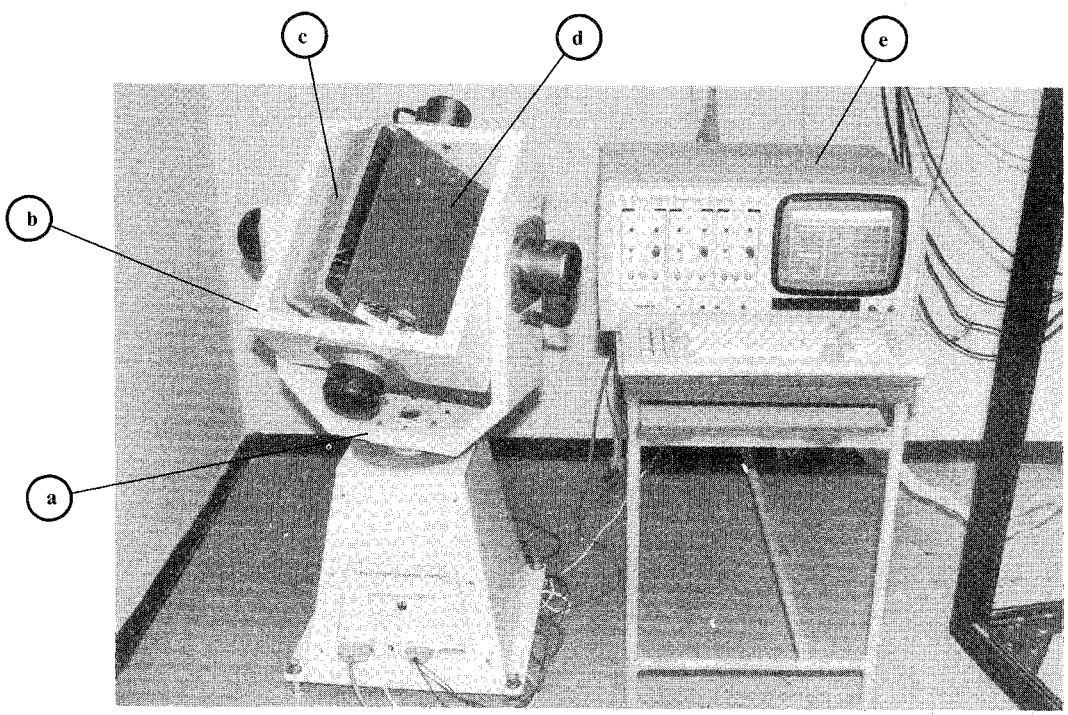

Fig. 5 Flight table: a) yaw gimbal; b) pitch gimbal; c) roll gimbal; d) triad of rate gyros; and e) digital controller.

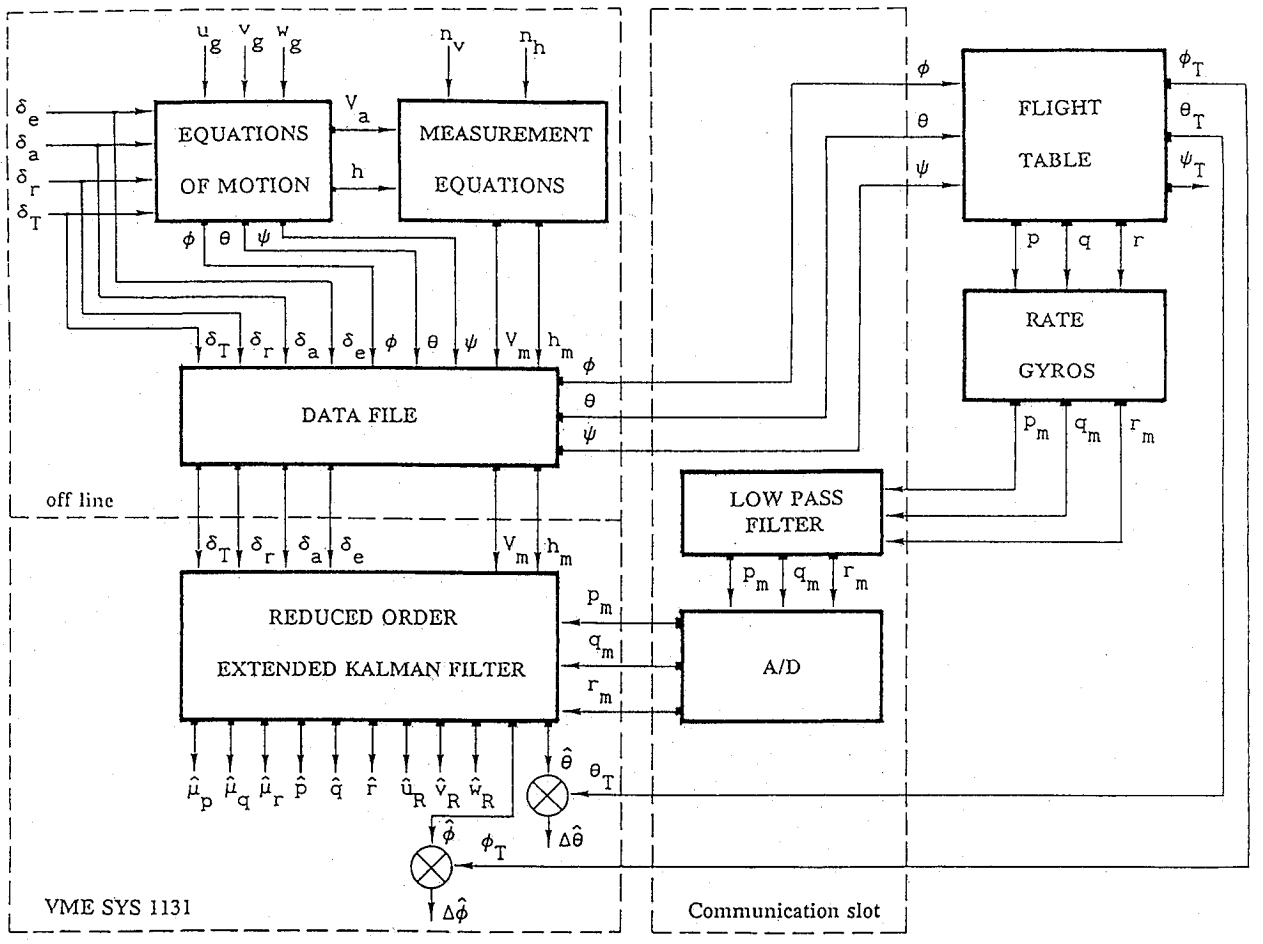

Fig. 6 Block diagram of experimental setup.

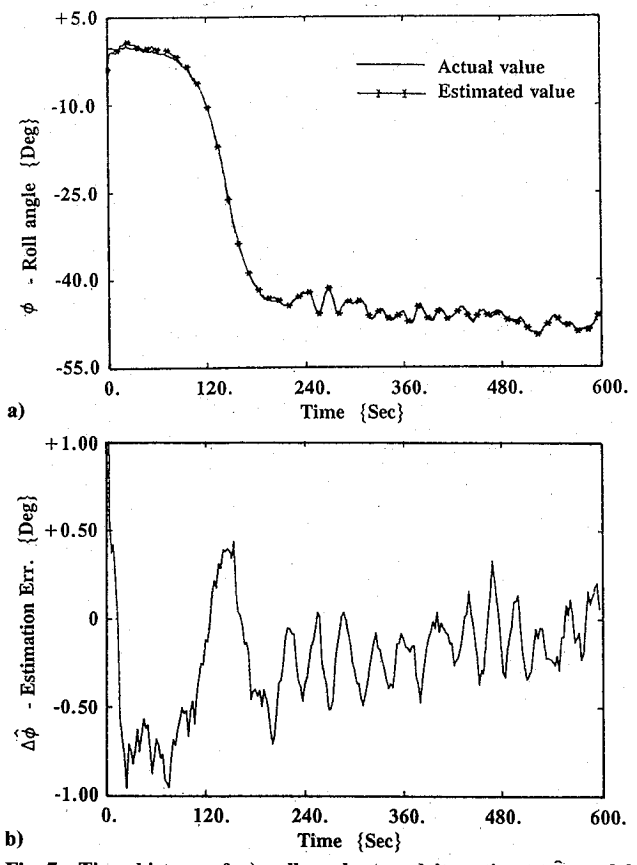

Fig. 7 Time history of a) roll angle ϕ and its estimate $\hat{\phi}$, and b) estimation error $\Delta\hat{\phi}$ using the reduced-order EKF in noncontrolled flight with real gyros on the flight table.

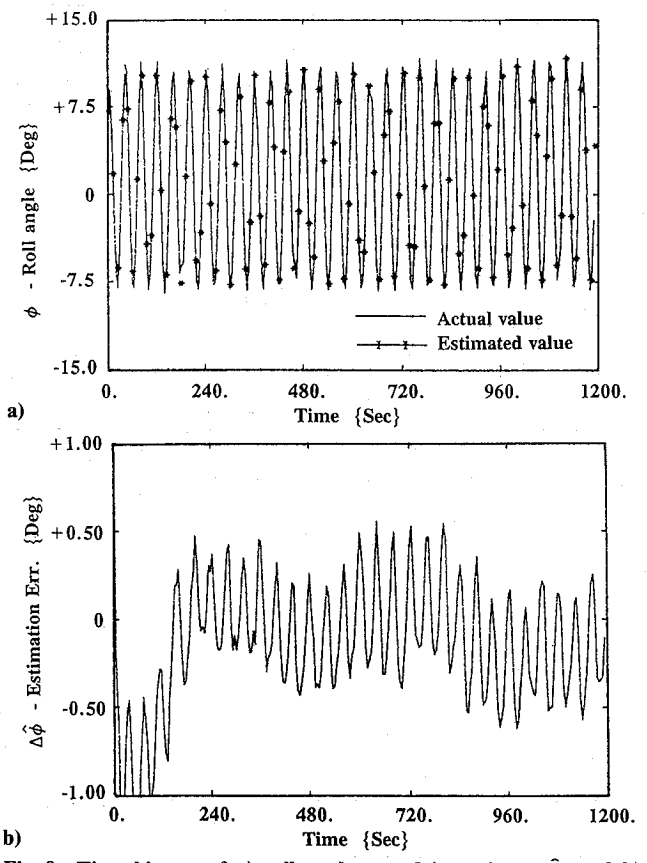

Fig. 8 Time history of a) roll angle ϕ and its estimate $\hat{\phi}$, and b) estimation error $\Delta\hat{\phi}$ using the reduced-order EKF in a "slalom" flight with real gyros on the flight table.

"slalom" flight under conditions identical to those of Fig. 4. Again, the errors are somewhat larger than the corresponding ones obtained for the computer simulations of Fig. 4. The results shown here are only a small sample of simulation tests that were performed. The overall conclusion from these tests is that, under all conditions, the estimation errors of attitude angles did not exceed 0.5 deg.

Conclusions

The study described herein, demonstrates that the measurement vector, typically provided by the set of state-of-the-art onboard sensors, is of sufficiently small dimension to permit on-line implementation of an extended Kalman filter (EKF) that provides accurate attitude estimates, meeting operational requirements without time limitation. The reduced-order multirate EKF is sufficiently robust under variations in aircraft model parameters and performs well under widely varying flight trajectories. With the advent of low-cost laser gyros[14] and fiber-optic or vibratory micromechanical gyros,[15] the concept described herein may evolve as a subminiature, highly reliable device.

Appendix A: Aircraft Equations of Motion

1) Dynamical translatory equations in body axes:

$$\dot{u} = -\tfrac{1}{2}\rho V_a^2\,(S/m)[C_D\cos\alpha\cos\beta + C_Y\cos\alpha\sin\beta - C_L\sin\alpha] + (T/m) - g\sin\theta - qw + rv \tag{A1}$$

$$\dot{v} = -\tfrac{1}{2}\rho V_a^2\,(S/m)[C_D\sin\beta - C_Y\cos\beta] + g\sin\phi\cos\theta - ru + pw \tag{A2}$$

$$\dot{w} = -\tfrac{1}{2}\rho V_a^2\,(S/m)[C_D\sin\alpha\cos\beta + C_Y\sin\alpha\sin\beta + C_L\cos\alpha] - g\cos\theta\sin\phi - pv + qu \tag{A3}$$

2) Dynamical angular equations in body axes:

$$\dot{p} = \left[1/\left(I_xI_z - I_{xz}^2\right)\right]\left\{I_z\left[\tfrac{1}{2}\rho V_a^2\,SbC_l + (I_y - I_z)qr\right] + I_{xz}\left[\tfrac{1}{2}\rho V_a^2\,SbC_n + (I_x - I_y + I_z)pq - I_{xz}qr\right]\right\} \tag{A4}$$

$$\dot{q} = \left[1/(I_y)\right]\left[\tfrac{1}{2}\rho V_a^2\,ScC_m + I_{xz}(r^2 - p^2) + (I_z - I_x)rp\right] \tag{A5}$$

$$\dot{r} = \left[1/\left(I_xI_z - I_{xz}^2\right)\right]\left\{I_x\left[\tfrac{1}{2}\rho V_a^2\,SC_n + (I_x - I_y)pq\right] + I_{xz}\left[\tfrac{1}{2}\rho V_a^2\,SbC_l + (I_y - I_x - I_z)qr + I_{xz}pq\right]\right\} \tag{A6}$$

3) Kinematical (Euler) equations:

$$\dot{\phi} = p + q\tan\theta\sin\phi + r\cos\phi\tan\theta \tag{A7}$$

$$\dot{\theta} = q\cos\phi - r\sin\phi \tag{A8}$$

$$\dot{\psi} = q\frac{\sin\phi}{\cos\theta} + r\frac{\cos\phi}{\cos\theta} \tag{A9}$$

4) Transformation of ground speed from body to Earth coordinates:

$$\dot{Z}_E = -\dot{h} = -u\sin\theta + v\sin\phi\cos\theta + w\cos\phi\cos\theta \tag{A10}$$

$$\dot{X}_E = u\cos\theta\cos\psi + v(\sin\phi\sin\theta\cos\psi - \cos\phi\sin\psi) + w(\cos\phi\sin\theta\cos\psi + \sin\phi\sin\psi) \tag{A11}$$

$$\dot{Y}_E = u\cos\theta\sin\psi + v(\sin\phi\sin\theta\sin\psi + \cos\phi\cos\psi) + w(\cos\phi\sin\theta\sin\psi - \sin\phi\cos\psi) \tag{A12}$$

5) Aerodynamic coefficients:

$$C_L = C_{L_o} + C_{L_\alpha}\alpha + C_{L_\beta}\beta + \frac{c}{2V_a}C_{L_q}q + C_{L_{\delta_e}}\delta_e \tag{A13a}$$

$$C_m = C_{m_o} + C_{m_\alpha}\alpha + C_{m_\beta}\beta + \frac{c}{2V_a}(C_{m_{\dot\alpha}}\dot\alpha + C_{m_q}q) + C_{m_{\delta_e}}\delta_e \tag{A13b}$$

$$C_D = C_{D_o} + C_kC_L^2 \tag{A13c}$$

$$C_Y = C_{Y_\alpha}\alpha + C_{Y_\beta}\beta + \frac{b}{2V_a}(C_{Y_p}p + C_{Y_r}r) + C_{Y_{\delta_a}}\delta_a + C_{Y_{\delta_r}}\delta_r + C_{Y_{\delta_e}}\delta_e \tag{A13d}$$

$$C_l = C_{l_\alpha}\alpha + C_{l_\beta}\beta + \frac{b}{2V_a}(C_{l_p}p + C_{l_r}r) + C_{l_{\delta_e}}\delta_e + C_{l_{\delta_a}}\delta_a + C_{n_{\delta_r}}\delta_r \tag{A13e}$$

$$C_n = C_{n_\alpha}\alpha + C_{n_\beta}\beta + \frac{b}{2V_a}(C_{n_p}p + C_{n_r}r) + C_{n_{\delta_e}}\delta_e + C_{n_{\delta_a}}\delta_a + C_{n_{\delta_r}}\delta_r \tag{A13f}$$

The absolute value of relative airspeed V_a, angle of attack α, and angle of sideslip β are given by

$$V_a = [(u-u_g)^2 + (v-v_g)^2 + (w-w_g)^2]^{1/2} \tag{A14a}$$

$$\alpha = \tan^{-1}\left[\frac{w-w_g}{u-u_g}\right] \tag{A14b}$$

$$\beta = \sin^{-1}\left[\frac{v-v_g}{V_a}\right] \tag{A14c}$$

The relationship between air density ρ and altitude h is given by

$$\rho = 352.90 \times \frac{\{1 - [h/(4.4\times10^4)]\}^{5.2067}}{288.15 - 6.5\times10^{-3}h} \tag{A15}$$

Appendix B: Extended Kalman Filter Equations

The state-space equation of the system is given by Eq. (1). The measurement equation is given by Eq. (2). The EKF, which provides the estimate $\hat{X}$ of X by means of Z, is derived as follows. Denote the estimation error by

$$x = X - \hat{X}$$

The algorithm is executed in the following steps.

1) Solve the differential equation

$$\dot{\hat{X}} = f(\hat{X}, U) \tag{B1}$$

from the instant t_k to t_{k+1}, where $\hat{X}(t_k) = \hat{X}_{k|k}$, and the solution at t_{k+1} will be denoted by $\hat{X}_{k+1|k}$.

2) Propagate the estimation error covariance matrix $P \triangleq E(XX^T)$ as

$$\dot{P} = F(\hat{X}, U)P + PF^T(\hat{X}, U) + Q(t) \tag{B2}$$

where

$$F(\hat{X},U) = \left.\frac{\partial f(X,U)}{\partial X}\right|_{X=\hat{X}_{k|k}} \tag{B3}$$

and $Q(t)$ is the power spectral density matrix of white system process noise

$$E\{W(t)W(t-\tau)\} = Q(t)\delta(t-\tau)$$

Equation (B2) must be solved from the instant t_k to t_{k+1}, where the initial condition is $P(t_k) = P_{k|k}$. The solution at the instant t_{k+1} will be denoted by $P_{k+1|k}$.

3) Compute the matrix K as

$$K_{k+1} = \mathrm{P}_{k+1|k}H^T[HP_{k+1|k}H^T + R_k]^{-1} \tag{B4}$$

where R_k is the covariance matrix of the measurement noise V_k.

4) Compute $\hat{x}_{k+1|k+1}$ by

$$\hat{x}_{k+1|k+1} = K_{k+1}[Z_{k+1} - H\hat{X}_{k+1|k}] \tag{B5}$$

and update $\hat{x}_{k+1|k+1}$ in accordance with

$$\hat{X}_{k+1|k+1} = \hat{X}_{k+1|k} + \hat{x}_{k+1|k+1} \tag{B6}$$

5) Update the covariance matrix P in accordance with

$$P_{k+1|k+1} = [I-K_{k+1}H]P_{k+1|k}[I-K_{k+1}H]^T + K_{k+1}R_kK_{k+1}^T \tag{B7}$$

Acknowledgments

This work was supported by the Department of Research and Development of the Israel Ministry of Defence and the Precision Instrument Industries, a subsidiary of Israel Aircraft Industries. Comments and insights given by I. Bar Itzhack of the Department of Aerospace Engineering are greatly appreciated. This paper is based on the M.Sc. thesis of the first author.

References

[1]Kayton, M., and Fried, W. R., *Avionic Navigation System,* Wiley, New York, 1972.

[2]Farrel, J. L., *Integrated Aircraft Navigation,* Academic Press, New York, 1976.

[3]Bar-Itzhack, I. Y., and Ziv, I., "Frequency and Time Domain Design of a Strapdown Vertical Determination System," AIAA Paper 86-2148, Aug. 1986.

[4]Craig, R. J. G., "Theory of Operation of Elastically Supported, Tuned Gyroscope," *IEEE Transactions on Aerospace and Electronic Systems,* Vol. AES-8, No. 3, 1972, pp. 280–288.

[5]Hill, M. L., "Introducing the Electrostatic Autopilot," *Astronautics and Aeronautics,* Vol. 10, Nov. 1972, pp. 22–31.

[6]Pietila, R., and Dunn, W. R., Jr., "A Vector Autopilot System," *IEEE Transactions on Aerospace and Electronic Systems,* Vol. AES-12, No. 3, 1976, pp. 341–347.

[7]Bryson, A. E., Jr., "Kalman Filter Divergence and Aircraft Motion Estimators," *Journal of Guidance and Control,* Vol. 1, No. 1, 1978, pp. 71–78.

[8]Grunwald, A. J., Wahnon, E., and Merhav, S. J., "Estimation of Vehicle Attitude and Flight-Path Angles from Low Cost Rate Gyro Measurements," *Proceedings of 25th Israel Annual Conference on Aviation and Astronautics,* Technion, Haifa, Israel, Feb. 1983, pp. 121–127.

[9]Sri-Jayanatha, M., and Stengel, R. F., "Determination of Nonlinear Aerodynamic Coefficients Using the Estimation-Before-Modeling Method," *Journal of Aircraft,* Vol. 25, No. 9, 1988, pp. 796–804.

[10]Etkin, B., *Dynamics of Atmospheric Flight,* Wiley, New York, 1972.

[11]Gelb, A., *Applied Optimal Estimation,* MIT Press, Cambridge, MA, 1974.

[12]Hinkley, D. V., "Inference About the Change Point from Cumulative Sum Tests," *Biometrika,* Vol. 58, No. 3, 1971, pp. 509–523.

[13]Basseville, M., et al., "Edge Detection Using Sequential Methods for Change in Level. Part II: Sequential Detection of Change in Mean," *IEEE Transactions on Acoustics, Speech and Signal Processing,* Vol. ASSP-29, No. 1, 1981, pp. 32–50.

[14]Killpatrick, J., and Weber, M., "The GG1308—A Small Low-Cost Electronic Gyroscope," AIAA Paper 86-2210, Aug. 1986.

[15]Boxenhorn, B., and Greiff, P., "A Vibratory Micromechanical Gyroscope," AIAA Paper 88-4177, Aug. 1988.